Hunting for the Active Sites of Surface-Enhanced Raman Scattering: A New Strategy Based on Single Silver Particles

Tong Xiao,[†] **Qi Ye, and Li Sun***

Department of Chemistry, University of Minnesota, Minneapolis, Minnesota 55455

Received: July 16, 1996; In Final Form: October 9, 1996[⊗]

Three major findings are reported here. First, a new technique based on lithographic modification with a scanning tunneling microscope (STM) has been developed for fabricating single Ag particles on atomically flat Au(111) surfaces. Second, surface-enhanced Raman scattering (SERS) from one isolated Ag particle has been observed and quantified for the first time. The enhancement factor due to one Ag particle of about 1 μm diameter is on the order of 10^4. This factor includes contributions from all forms of chemical enhancement, which are smaller than 10^2. Finally, strong evidence suggests the importance of clusters containing closely-spaced particles. Extra enhancement due to clusters of randomly distributed Ag particles is around 10^2. We believe that the extra enhancement is spatially localized near the gap sites between two particles in proximity. These gap sites form an important class of SERS-active sites.

Introduction

We report here a new strategy for revealing the correlation between the surface morphology of a SERS substrate and the corresponding enhancement factor. The key of this strategy involves fabrication and characterization of single Ag nanoparticles on an atomically flat surface through a combined use of three techniques: scanning probe microscopy, electrochemistry, and surface Raman spectroscopy. The new strategy has already allowed us to observe SERS from one single Ag particle and to gain a useful insight into the role of interparticle interactions. We believe that this work points to a promising new direction for quantitatively evaluating the importance of various competing SERS mechanisms.

Since the discovery of SERS about 20 years ago,[1,2] many theories have been proposed to explain this phenomenon which involves nearly a million-fold enhancement of the Raman scattering cross section for molecules adsorbed on the surface of metal nanoparticles.[3−6] Two major types of enhancement are now recognized: the long-range electromagnetic (EM) field enhancement[7,8] and the short-range chemical enhancement.[9,10] Since the chemical enhancement does not require the presence of nanoparticles, it can be studied independently using atomically flat surfaces.[11,12] However, verifying the predictions of an EM theory has been difficult because it is difficult to fabricate stable and well-defined SERS-active surface morphology.[13−20] To solve this problem, several new methods for producing roughened surfaces have been developed.[21−26] For example, silver-coated latex spheres as well as immobilized monodispersed colloidal particles are morphologically more stable than an electrochemically roughened surface.[14,15,24]

Although the stability is improved, the above substrates are still not ideal for probing the SERS mechanisms. For example, a silver overlayer on latex spheres has a complex geometry which may not be amenable to theoretical modeling. The size of monodispersed colloidal particles is limited to be less than 100 nm, and the control of interparticle spacing is far from ideal.[25] More importantly, in the above two examples, the detected SERS signal results from a large number of particles; thus, interparticle interactions cannot be easily eliminated or accurately quantified, especially when the spatial distribution of a particle ensemble is random. Interparticle interactions are more defined in arrays of regularly-spaced particles fabricated either by photolithography or by template methods.[27−30] However, the particle density reported so far may be still too high to completely avoid the effects of interparticle interactions and to isolate the intrinsic enhancement due to individual particles.

Obviously, for mechanistic studies it is desirable to observe SERS from one single particle. Toward this goal, Van Duyne and Haller have developed a SERS microprobe.[31,32] However, the detection efficiency of their PMT/scanning spectrometer setup was inadequate. In addition, at the time of their investigation, techniques for fabricating and characterizing single particles were neither well-developed nor widely available. We have overcome all of these technical difficulties in this study, thus observed SERS from one single particle for the first time.[33]

Experimental Section

Chemicals and Materials. Water of 18.2 MΩ cm resistivity (Milli-Q Plus, Millipore) was used in all electrochemical measurements. *n*-Hexadecanethiol (distilled twice from a 92% product before use), phosphorus tribromide (99%), thiourea (99+%), and *trans*-4-stilbenemethanol were obtained from Aldrich Chemical Co. Silica gel (J. T. Baker Inc.) and organic solvents of reagent grade or better were used as received.

Synthesis of *trans*-4-Mercaptomethyl Stilbene. *trans*-4-Mercaptomethyl stilbene (*t*-4MMS) was synthesized via a thiouronium intermediate $PhCH{=}CHPhCH_2SH$.[34] Transformation via the thiolacetate intermediate was also attempted, but the yield was lower (10%).[35]

***trans*-4-Bromomethyl Stilbene (1).** To a stirred solution of *trans*-4-stilbenemethanol (0.43 g, 2 mmol) in CH_2Cl_2 (50 mL) was added phosphorus tribromide (0.32 g, 1.18 mmol) in CH_2Cl_2 (20 mL). After reaction at 0 °C under N_2 for 10 h, the mixture was quenched by 100 mL of water. The organic layer was washed sequentially with 5% $NaHCO_3$ (50 mL) and brine

---

[†] Present address: Department of Chemistry, University of Rochester, Rochester, NY 14627.

[*] Author to whom correspondence should be addressed. E-mail: sun@chemsun.chem.umn.edu.

[⊗] Abstract published in *Advance ACS Abstracts,* January 1, 1997.

S1089-5647(96)02135-9 CCC: $14.00

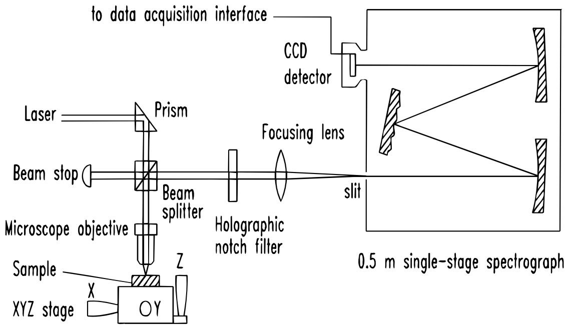

Figure 1. Schematic diagram of the Raman microscopic system.

(100 mL). Drying over $CaCl_2$ and removal of the solvent gave 0.44 g of crude product. Elution on a silica gel column with *n*-hexane/chloroform (6:1) yielded 0.43 g (80%) of **1** as a white powder: ^1H NMR ($CDCl_3$) δ 7.4−7.5 (m, 9H), 7.1 (d, 2H), 4.5 (s, 2H).

***trans*-4-Mercaptomethyl Stilbene (2).** A mixture of **1** from the above step, thiourea (0.12 g, 11.6 mmol) in degassed ethanol (75 mL) was stirred under N_2 for 9 h at room temperature. After solvent removal, the remaining white solid (a thiouronium salt) was refluxed in a degassed solution of NaOH (0.13 g, 3.12 mmol; 50 mL water) for 5 h. The reaction mixture was cooled to 0 °C, acidified to pH 2 with 6 N HCl, extracted with chloroform (2 × 40 mL), and dried over $MgSO_4$. Flash chromatography (5:1 *n*-hexane/chloroform) afforded 0.17 g (47%) of **2** as a white solid: ^1H NMR [$(CD_3)_2SO$] δ 7.6−7.3 (m, 9H), 7.2 (d, 2H), 3.7 (d, 2H), 2.9 (t, 1H); Raman (647.1 nm excitation) 2561 cm^{-1} (S−H stretching vibration).

Surface Raman Spectroscopy. The electrochemical and Raman spectroscopic measurement systems have been described previously.[36] The Raman system was modified slightly to adapt to the present work (Figure 1). A 10×, 0.21 NA microscope objective (Nikon) was installed to focus the laser to a diffraction-limited spot at a 0° incident angle. The same objective was also used to collect Raman photons via a cube beam splitter (Edmond Scientific, Barrington, NJ). Routine data acquisition parameters were 400 μm slit width, 2 mW laser power, and 50 s integration time. Samples were moved relative to the laser spot with an *xyz* translational stage (Newport, Irvine, CA) of 0.5 μm resolution.

Scanning Probe Microscopy. All STM and scanning force microscopic (SFM) images were acquired with a Nanoscope III microscope (Digital Instruments, Santa Barbara, CA). Vibration isolation was accomplished with the "bungee"-cord design.[37]

The STM tips were mechanically cut from a 0.010-in. diameter Pt/Ir (80/20 w/w) wire while the SFM tips were pyramidal silicon nitride cantilevers with a spring constant of 0.58 N/m. Typical STM imaging conditions were 300 mV bias voltage, 0.11 nA constant tunneling current, and 2 Hz scan rate. Constant force mode and a 2-Hz scan rate were used in SFM imaging, but the exact force was unknown because the force-vs-distance plot was not recorded.

Typical conditions for STM lithography were 3−5 V bias voltage, 0.11 nA tunneling current, 30−40 Hz scan rate, and 3 min etching time.[38,39] All the STM lithographic operations were performed in air without humidity control although we found later that humidity is a critical factor.[40]

Sample Preparation and Measurements. Au(111) facets on an Au sphere were prepared according to literature procedures.[38−42] The remaining fabrication steps are illustrated in Figure 2. Ag particles with adsorbed probe molecules were first characterized by SERS, and then by SFM. A home-made sample holder, similar to a previous design,[42] was used to aid sample transfer between three major instruments, namely, the potentiostat, the Raman spectrograph, and the scanning probe microscope.

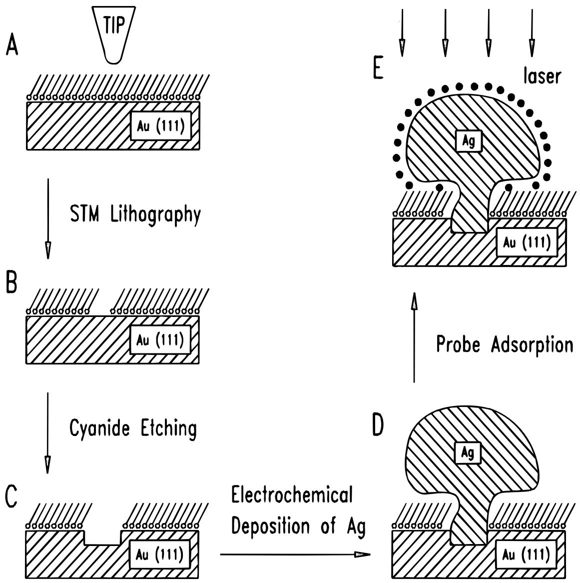

Figure 2. Fabrication of single Ag particles for SERS measurements. A self-assembled monolayer (SAM) of hexadecanethiol (open circles with linear tails) on Au(111) was prepared by soaking an Au sample in a 1 mM ethanolic thiol solution for 48 h. The SAM resist was patterned via STM lithography and then developed further by electrochemical anodization in a solution of 0.1 M Na_2HPO_4 and 0.1 M NaCN at 300 mV (vs an Ag/AgCl/3 M NaCl reference electrode) for 10 s. After transfer to another electrolyte containing 1 mM $AgClO_4$ and 0.1 M $HClO_4$, a single Ag particle was deposited onto the lithographic window at 470 mV (vs an Ag/AgCl/saturated-KCl/0.1 M $HClO_4$ reference electrode) for 3 min. The Ag particle was covered with a SAM of Raman probe (solid filled circles) after soaking in an ethanolic solution of *t*-4MMS for 20 min.

Results and Discussion

A. Fabrication and Analysis of Single Ag Particles

Cyanide Etching and Silver Deposition by Electrochemical Methods. Initially, we hoped to use STM lithography to create a microeletrode and grow one Ag particle from it. However, this approach was not successful because there was not enough contrast between the Ag deposition rate at the tip-etched area and the rates elsewhere. We noticed that the threshold potential for Ag deposition onto etched areas varied randomly for different samples from 0 to 400 mV, a range more negative than the theoretical threshold of 425 mV for bulk deposition from a 1 mM Ag^+ solution. This suggests that the thiols in tip-etched area have not been completely removed, which would lead to large, and perhaps irreproducible, threshold overpotential. One consequence of large overpotential is that Ag is also deposited at the adventitious defect sites. We have attempted to remove the residue thiols in the tip-etched area by oxidizing it at 1100 mV prior to Ag deposition.[43] However, this anodic excursion enhances Ag nucleation at the adventitious defects as well, resulting in no or even decreased contrast in Ag deposition rate (Figure 3). The Ag particle density is so high that it is impossible to find features due to STM lithography.

We then tried to remove the thiol residue through electrochemically controlled cyanide etching. Unlike Ag deposition, cyanide etching exhibits a large contrast in etching rate: no pits are observed in the area not etched by the STM tip. Consequently, cyanide etching dramatically improves the con-

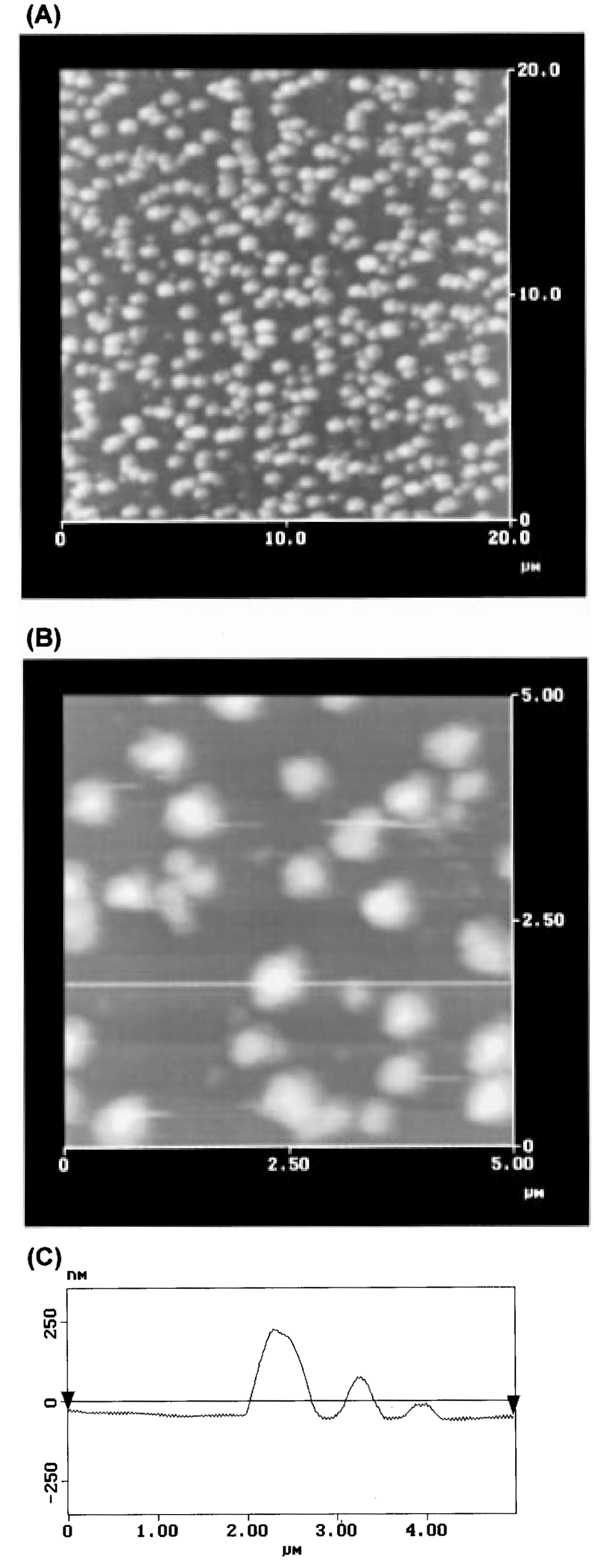

Figure 3. (A) SFM image of clusters of Ag particles deposited onto adventitious defect sites within a hexadecanethiol SAM on Au(111). The deposition potential was 200 mV, and the deposition time was 10 s. (B) Smaller scan area. (C) Line profile shown in B. The *z* scale in both A and B is 500 nm.

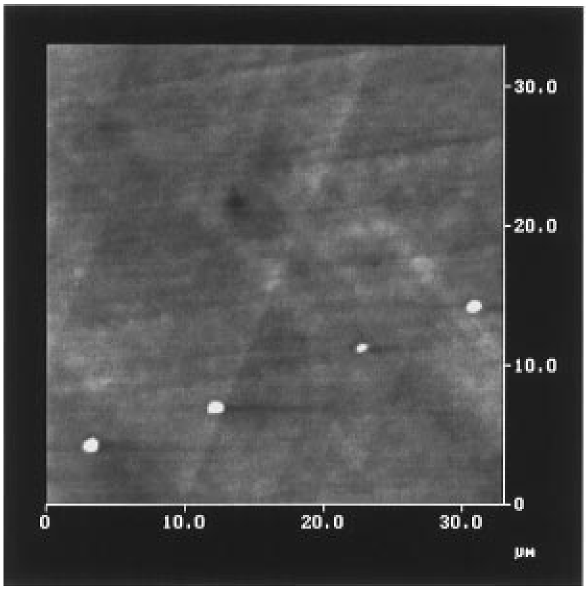

Figure 4. SFM image of a string of mesa-like Ag deposits at four tip-etched and cyanide-cleaned 1 µm × 1 µm windows. Ag was deposited at 500 mV for 20 s. The *z*-scale is 10 nm.

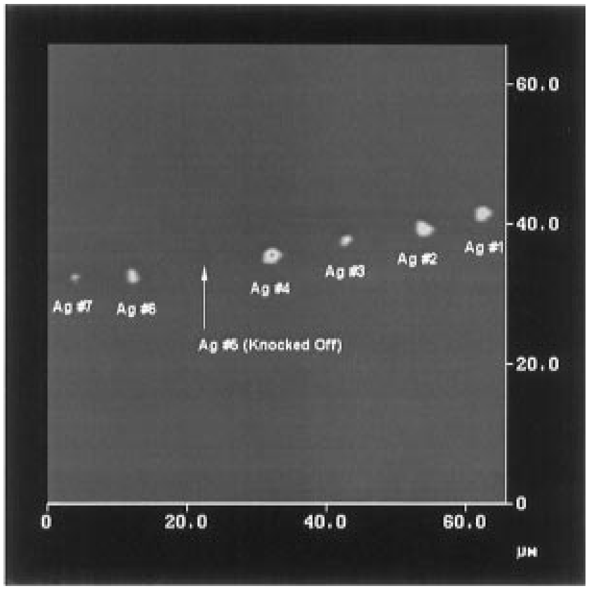

Figure 5. SFM image of a string of Ag particles deposited at seven tip-etched and cyanide-cleaned 500 nm × 500 nm windows. Ag was deposited at 470 mV for 3 min. The *z*-scale is 1 µm. The Ag#5 particle was knocked off the surface by the imaging SFM tip.

trast in the Ag deposition rate. There exists a window of threshold potential within which Ag deposition occurs at the tip-etched, cyanide-cleaned area but not at the adventitious defect sites. Figure 4 shows an SFM image of Ag particles produced with this method. At a full *z*-scale of 10 nm, no Ag particles can be seen in the area not etched by the STM tip. Longer deposition time simply results in a larger particle size (Figure 5).[44]

Size and Shape Analysis of Ag particles. As seen in Figure 6, a close-up view of an individual particle does not reveal its true topography because the SFM tip has a finite cone angle.[45,46] According to a simple geometrical model, α' obtained from a line cross section should be equal to α, the half cone angle of the pyramidal SFM tip (Figure 7). The calculated half cone angle is 35°, assuming that each face of the pyramid is molded from a Si(111) plane.[47] This agrees approximately with the observed α' of 32° ± 3° obtained from line cross sections, such as the one shown in Figure 6B.

The relatively dull SFM tip makes it difficult to determine the shape of each particle. Nevertheless, an Ag particle may be approximated as a spherical protrusion with its center located at a distance *q* away from the Au surface (Figure 7). The

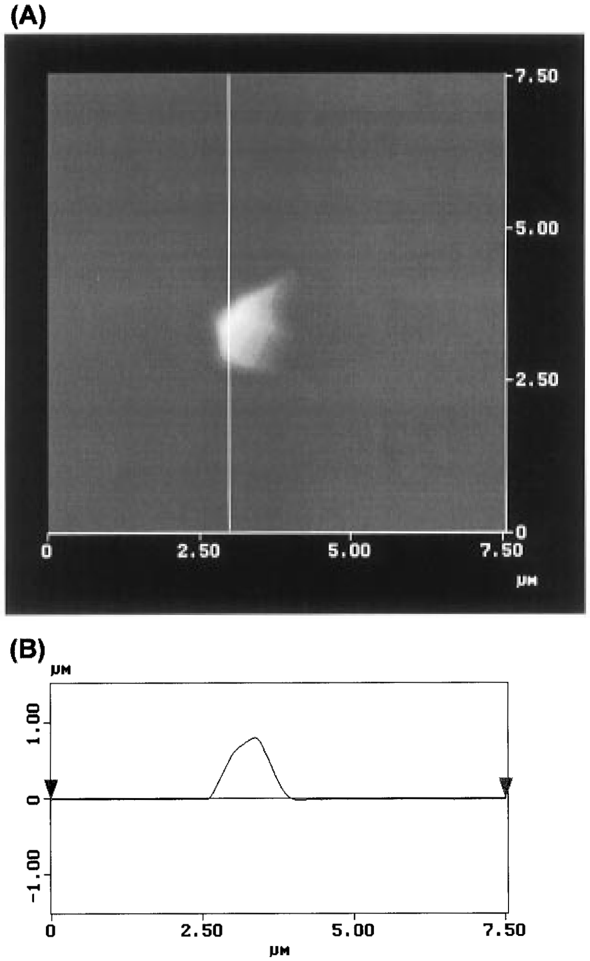

Figure 6. SFM image and a line profile of the Ag#3 particle shown in Figure 5. The *z*-scale in A is 2 μm.

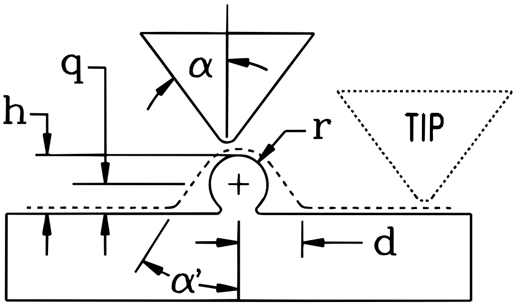

Figure 7. Illustration of a spherical particle being imaged by a pyramidal SFM tip. The dashed line represents the observed topography. Symbols are defined in the text.

motivation behind this model is to obtain the radius of curvature, a parameter of great significance in characterizing the roughness scale of a SERS-active substrate. After a simple derivation based on geometric algebra, we obtain an equation which relates the radius of curvature r with three parameters that can be conveniently determined from an SFM image, namely, the half base width d, the height h, and the cone angle α':

$$r = \frac{1}{1 - \sin\alpha}(d\cos\alpha - h\sin\alpha) - r_{\mathrm{tip}} \qquad (1)$$

where $\alpha = \alpha' = \arctan(d/h)$. Since the tip radius of curvature r_{tip} is much smaller than the particle's radius, the last term can be ignored. The value q ($q = h - r$) gives us a rough estimate of particle shape. For example, $h = 2r$ and $q = r$ correspond to a sphere whereas $h = r$ and $q = 0$ correspond to a hemisphere.

The radius obtained with eq 1 is subject to a large uncertainty, however. On the basis of sequential images of the same particle, we observed a 5% error in h and d, and a 10% error in α'. Error propagation results in even larger error in radii. For example, the Ag#3 particle in Figure 5 shows $r = 370 \pm 110$ nm and $q = 420 \pm 120$ nm; the Ag#4 particle shows $r = 590 \pm 120$ nm and $q = 450 \pm 130$ nm. Thus, these particles are approximately spherical ($r \approx q$) although the geometry below the top hemisphere cannot be obtained from an SFM image. Similar analysis of the Ag particles in Figure 3B reveals a hemispherical shape with typical $r = 310 \pm 66$ nm and $q = -30 \pm 70$ nm. The hemispherical shape is reasonable since, in this case, Ag was deposited under a large overpotential that favors diffusion-controlled growth.[48]

Discussions on the Single Particle Fabrication Technique. The single particle fabrication technique outlined here has three distinct advantages for SERS mechanistic studies. First, this technique allows unambiguous isolation of a single particle for SERS measurements. The region surrounding each particle is an atomically flat Au(111) surface which is known to support little or no EM enhancement. Furthermore, Raman probe molecules are excluded from the flat Au(111) region which has been protected with the SAM of hexadecanethiol. In short, any Raman signal from the probe molecules originates from the surface of one isolated Ag particle. This kind of isolation is important since the laser spot size is usually larger than the particle size, which means that it is inevitable that a significant portion of laser energy will be incident on the surface surrounding the particle (*vide infra*). Second, the size and the shape of the particle can be controlled by controlling the size and the shape of the lithographic area and by controlling the Faradaic charge passed during the Ag deposition step. Due to the high spatial resolution of STM lithography, we expect that particles as small as 10 nm can be fabricated and characterized. Finally, the interparticle spacing, thus the degree of interactions among the localized EM field around each particle (*vide infra*), can also be controlled by controlling the etched pit spacings during STM lithography. In this study, we have demonstrated only the first advantage.

Combining electrochemistry and scanning probe microscopy for fabricating and characterizing nanometer-scale features is a very useful concept that has been demonstrated in this work and elsewhere.[38,49−51] For example, Li *et al.* reported a method for depositing Ag nanoparticles on an atomically flat graphite surface.[50,51] This method also has the aforementioned three advantages; therefore, it is potentially useful for single-particle SERS studies as well. One drawback is that the laser beam may overheat the graphite surface and cause various problems such as heat-induced desorption or morphology changes.

Since STM lithography relies on sequential tip movement to create patterns, its throughput is lower than those of parallel lithography based on masks,[52,53] stamps,[54,55] or templates.[29,56] However, the spatial resolution of STM lithography is much higher, and it is less prone to dust particle contamination. These are desirable characteristics for single particle fabrication which only demands low-throughput operations.

B. Surface-Enhanced Raman Scattering from Single Ag Particles

Basic Equations of Surface Raman Spectroscopy. Quantitative analysis of SERS is the key to a better understanding of the SERS mechanisms. The integrated surface Raman intensity I_{SR} in photon s^{-1} can be expressed as[3]

$$I_{\mathrm{SR}} = \sigma'_{\mathrm{SR}}\Omega n_{\mathrm{S}} P_{\mathrm{L}} \eta \qquad (2)$$

where σ'_{SR} is the differential surface Raman scattering cross section in $cm^2\ sr^{-1}\ molecule^{-1}$; Ω is the solid angle of the collecting lens; n_s is the surface coverage in molecule cm^{-2}; P_L is the incident laser power in photon s^{-1}; and η is the overall detection efficiency which includes the transmission efficiency of the imaging optics and the quantum yield of the CCD detector.[57] Similarly, the normal Raman intensity I_{NR} from bulk molecular scatters embedded in a thin and transparent film is

$$I_{NR} = \sigma'_{NR}\Omega n_F P_L \eta \qquad (3)$$

where $\sigma'_{NR}$is the differential normal (or unenhanced) Raman scattering cross section and n_F the number of molecules per geometric area of the thin film.

The surface enhancement factor K_{EF} is defined as

$$K_{EF} = \frac{\sigma'_{SR}}{\sigma'_{NR}} = \frac{I_{SR}n_F}{I_{NR}n_S} = \frac{I_{SR}}{\sigma'_{NR}\Omega n_S P_L \eta} \qquad (4)$$

where Ω, η, and P_L are all assumed to be constants for both surface and bulk measurements. If σ'_{NR} is unknown, it can be determined by comparing its Raman intensity with a standard sample whose σ'_{NR} is known:

$$\sigma^{B}_{NR} = \frac{I^{B}_{NR}n^{A}_{F}}{I^{A}_{NR}n^{B}_{F}}\sigma^{A}_{NR} \qquad (5)$$

Again, Ω, η, and P_L should be kept constant. To ensure a constant η, the frequencies of the two Raman lines should be near each other.

Typical parameters used in this study are $\eta = 1.7 \times 10^{-3}$ according to eq 3,[58] $\Omega = \pi NA^2/(1 - NA^2) = 0.145$,[59] $\sigma'_{NR} = 2.7 \times 10^{-28}\ cm^2\ sr^{-1}$ for the C=C stretching vibrations of the probe molecule (t-4MMS) according to eq 5,[60] and $n_S = 4.61 \times 10^{14}$ molecules/cm^2 for a closely-packed SAM of t-4MMS.[61] When calculating the enhancement factor due to one single particle using eq 4, one has to realize that the effective laser power is much smaller than the actual power. This is because the laser beam size is often larger than the size of a single particle. The correction factor can be found numerically if we assume that the particle is at the center of the beam and that the beam has a TEM$_{00}$ Gaussian cross section at its focal plane:[32]

$$I(r) = \frac{2P_L}{\pi r_0^{\ 2}}\exp(-2r^2/r_0^{\ 2}) \qquad (6)$$

where P_L is the total laser power. The measured spot radius r_0, defined as the radial distance at which the intensity falls to e^{-2} of the value at the center, is $4.3 \pm 0.2\ \mu m$.[62]

Correlation between Enhancement Factor and Particle Morphology. Under optimized experimental conditions, we did not observe surface Raman signal from any Ag particle shown in Figure 4. These particles, having a width of about 1.1 μm and a height of about 10 nm, resemble a "mesa" structure. The null detection does not imply no enhancement; rather, there exits an upper enhancement limit which is primarily determined by the detection efficiency η. After considering the correction factor for the incident power (about 4%), we find that the upper limit of the enhancement factor is about 250.[63] This value probably results from chemical enhancement alone since most mesa surface is "flat" (about 1 nm RMS roughness). EM enhancement at this roughness scale may also be possible, but its contribution, capped by 250, is still insignificant when compared with a typical overall enhancement of 1×10^6.

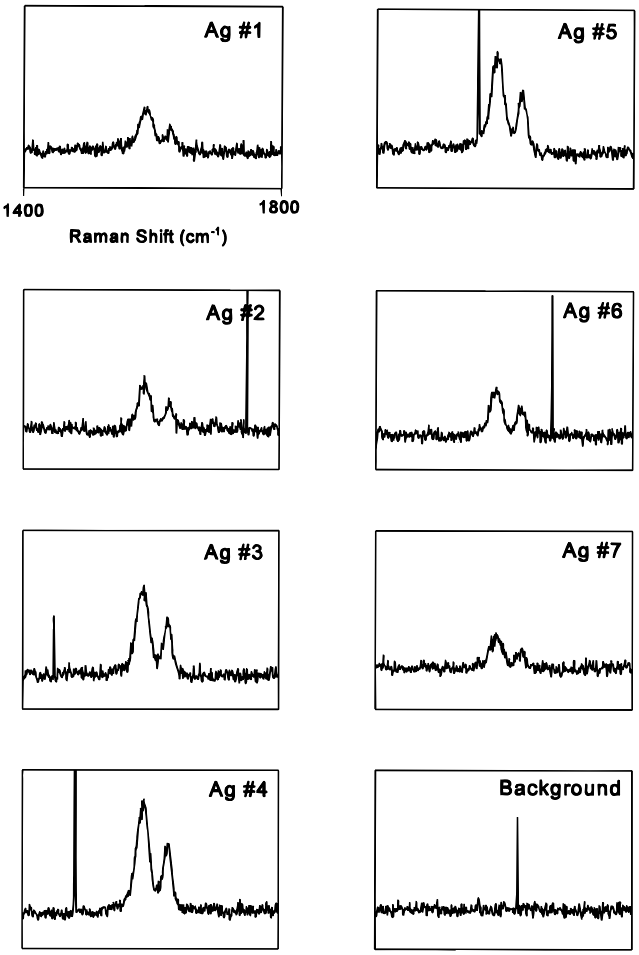

Figure 8. SERS spectra of t-4MMS adsorbed on the single Ag particles shown in Figure 5. The height of each box represents an intensity scale of 10 counts per second per mW of incident laser power. The background spectrum was obtained at a particle-free spot: around the lower-right corner of the image in Figure 5.

Figure 8 shows the surface Raman spectra obtained from individual Ag particles depicted in Figure 5. The bands at 1587 and 1626 cm^{-1} can be assigned to the phenyl ring C=C stretching vibration and the ethylene C=C stretching vibrations, respectively.[64] Although weak, the signals are clearly distinguishable from the background noise. Since the Ag particles are of different sizes, their SERS intensities also differ. Smaller diameter usually gives smaller intensity; however, exceptions to this trend are obvious, such as the case of Ag#3 vs Ag#1, indicating that the shape factor or the local roughness may be the causes.

Using eq 4, we can now estimate the enhancement factor due to one single Ag particle.[65] For example, the enhancement factor is 3.5×10^4 for the Ag#3 particle and 1.9×10^4 for the Ag#4 particle. These values include contributions from all forms of chemical as well as EM enhancement due to local roughness at a much smaller scale than the particle size. However, these contributions are less than 250 as discussed shortly before.

The above enhancement factors for single Ag particles are 2 orders of magnitude lower than the value measured with an Ag electrode roughened electrochemically.[3] We have initially attributed this discrepancy to the nonideal shape of the Ag particle. The Ag #3 particle has an aspect ratio of about 1 whereas a typical EM theory predicts that an ideal Ag particle should be an ellipsoid with an aspect ratio larger than 1.[66] However, a more careful analysis of our data obtained with

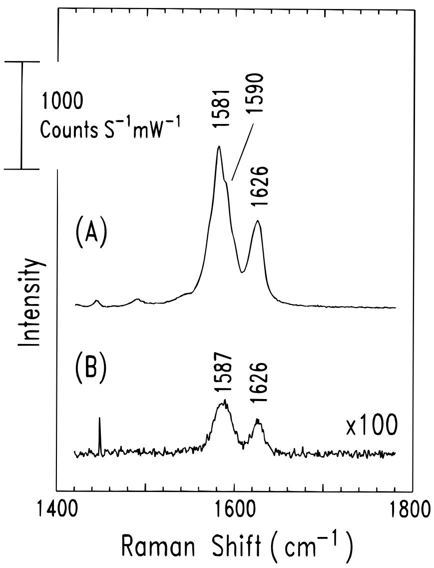

Figure 9. (A) Typical SERS spectrum of *t*-4MMS adsorbed on randomly distributed Ag particles shown in Figure 3. (B) SERS spectrum of *t*-4MMS adsorbed on the Ag#3 particle shown in Figure 5. The *y*-scale is magnified 100-fold.

another sample revealed something that demands a more critical examination of the above interpretation.

The sample of interest is the one shown in Figure 3, in which a much higher Ag particle density can be seen. The shape of these particles is hemispherical, which is probably less ideal than a spherical shape. However, the SERS signal from this sample is much more intense than the signal from one single particle, even if one includes the factor that more than one particles are illuminated by the focused laser beam (Figure 9).

Our suspicion is verified after a quantitative calculation of the enhancement factor. Since the average particle density does not change significantly over an area defined by the laser beam size, we can use an effective surface coverage given by

$$n_S = 2\pi r^2 n_{MONO} N_P \tag{7}$$

where $2\pi r^2$ is the surface area of a hemispherical particle; n_{MONO} is the closely-packed monolayer coverage; and N_P is the average particle density. Both r (average of 0.3 μm) and N_P (1.1×10^8 particles/cm^2) can be readily measured from Figure 3. Using eq 4, we can show that the enhancement factor is 1.1×10^6, which is about 60 times larger than the average enhancement factor of 1.9×10^4 for a single Ag particle of comparable size.

This result means that the SERS signal due to a cluster of closely-spaced particles is not simply the sum of signals from each individual particles. Rather, an extra enhancement due to interactions between these particles is present. We think the interactions involve perturbation of the local EM fields surrounding individual particles. This view has been speculated previously based on the effects of colloid aggregation on SERS.[18,27,28,67,68] For example, Blatchford *et al.* observed that SERS intensity from pyridine adsorbed on Au colloidal particles increases as the degree of aggregation increases.[67] They attributed this phenomenon to the excitation of the longitudinal EM resonance of string-like clusters, which produces an intense red-shifted absorption band near 650 nm.

However, previous experimental evidence is only qualitative evidence since the enhancement factor due to one isolated particle is virtually unknown. In previous SERS studies, the observed SERS signal results from a large number of particles which always include clusters; therefore, separating the contribution of isolated particles from that of clusters is difficult. Our single particle SERS experiments avoid this difficulty and make quantitative evaluations possible. Furthermore, we have shown a one-to-one correlation between the observed Raman signal from a single particle and its high-resolution topographical image. Therefore, the statistical averaging effect present in previous investigations[14−17,24,27] is completely avoided.

Intuitively, we believe that maximum perturbation of the local EM field occurs at the "gap sites" where molecules are flanked by two particles. This hypothesis agrees with the theoretical results by Gersten and Nitzan who showed that molecules located between a two-sphere cluster experience a stronger local EM field and resonance at a lower frequency than those for a single sphere.[69] Thus, these "gap sites" are an important class of SERS-active sites. With further refinement of our single particle technique, we will fabricate two-particle clusters which will allow direct comparison with the Gersten and Nitzan model.

Not every EM theory gives the same prediction for the effects of particle clustering. For example, Laor and Schatz showed that a cluster of hemispheroids on a perfect conductor will give a smaller enhancement factor and a broader resonance profile than those for a single particle.[70] Although a broader profile has supporting experimental evidence,[71] the smaller enhancement factor clearly contradicts to our observation.

This inconsistency, however, may not necessarily imply a fundamental difference between Laor and Schatz's theory and Gersten and Nitzan's theory. For example, besides the obvious difference in the geometric configurations of their models, Laor and Schatz averaged the EM field over the entire particle surface while Gersten and Nitzan focused only on the special site between two particles. This implies that the EM enhancement is not uniformly distributed around a particle surface and that the special "gap sites" are far more important than other sites in determining the overall enhancement factor. Our observation of the extra enhancement by clusters concurs with this picture qualitatively. Obviously, more quantitative comparisons will require refinements in both theoretical and experimental cluster geometries so that they converge to a common one.

Conclusions

We have demonstrated here a new technique for fabricating single Ag nanoparticles. The technique shows great potential for controlling the size, the shape, and the spatial configuration of model SERS particles.

We have detected for the first time surface-enhanced Raman scattering due to one isolated single Ag particle. The total enhancement factor due to one single Ag particle of about 1 μm diameter is about 10^4, which includes contributions from all forms of chemical and EM enhancement at roughness scales smaller than the dimension of the particle.

Finally, we quantitatively evaluated the role of interparticle interactions in SERS. Extra enhancement of about 60 is possible for Ag clusters of random spatial configuration. We speculate that the extra enhancement is due to the modulation of the local EM fields from individual particles. In particular, the gap sites between two particles may be more important to SERS than other sites. This possibility is significant because it will provide a valuable guideline for optimizing the surface morphology, thus the enhancement factor, of a practical SERS substrate. After further refinement, the single particle fabrication technique presented here should lead us to a more quantitative understanding of SERS-active sites.

Acknowledgment. L.S. gratefully acknowledges financial support from National Science Foundation (CHE-9531243). This work was initially supported by the University of Minnesota in the form of start-up funds. We thank Professor Timothy Lodge for loaning us a high precision translational stage and Mr. Mengcheng Chen for assistance in SFM imaging.

References and Notes

(1) Jeanmaire, D. L.; Van Duyne, R. P. *J. Electroanal. Chem.* **1977**, *84*, 1−20.

(2) Albrecht, M. G.; Creighton, J. A. *J. Am. Chem. Soc.* **1977**, *99*, 5215−5217.

(3) Van Duyne, R. P. In *Chemical and Biochemical Applications of Lasers*; C. B. Moore, Ed.; Academic Press: New York, 1979; p 101

(4) *Surface Enhanced Raman Scattering*; R. K. Chang, T. E. Furtak, Eds.; Plenum Press: New York, 1982.

(5) Otto, A. In *Light Scattering in Solids*; M. Cardona, G. Guntherodt, Eds.; Springer-Verlag: Heidelberg, 1984; p 289.

(6) Moskovits, M. *Rev. Mod. Phys.* **1985**, *57*, 783.

(7) Schatz, G. C. *Acc. Chem. Res.* **1984**, *17*, 370−376.

(8) Kerker, M. *Acc. Chem. Res.* **1984**, *17*, 271−277.

(9) Ueba, H. *Surf. Sci.* **1983**, *131*, 347−366.

(10) Otto, A. *J. Raman Spectrosc.* **1991**, *22*, 743−752.

(11) Campion, A.; Ivanecky, J. E., III; Child, C. M.; Foster, M. *J. Am. Chem. Soc.* **1995**, *117*, 11807−11808.

(12) Campion, A. *J. Electron Spectrosc. Relat. Phenom.* **1983**, *29*, 397−400.

(13) Here, the surface morphology refers to the size, shape, and spatial distribution of metal particles that are either supported on a substrate, such as Ag islands on a glass slide, or merged with a substrate, such as protrusions on an electrochemically roughened electrode surface. A related term, namely, "surface roughness", has a more narrow meaning: it only defines an average particle size and does not necessarily include a connotation of spatial distribution.

(14) Van Duyne, R. P.; Hulteen, J. C.; Treichel, D. A. *J. Chem. Phys.* **1993**, *99*, 2101−2115.

(15) Schueler, P. A.; Ives, J. T.; DeLaCroix, F.; Lacy, W. B.; Becker, P. A.; Li, J.; Caldwell, K. D.; Drake, B.; Harris, J. M. *Anal. Chem.* **1993**, *65*, 3177−3186.

(16) Roark, S. E.; Rowlen, K. L. *Anal. Chem.* **1994**, *66*, 261−270.

(17) Otsuka, I.; Iwasaki, T. *J. Vac. Sci. Technol. A* **1990**, *8*, 530−533.

(18) Sun, L. Ph.D. Thesis, Northwestern University, Evanston, IL, 1990.

(19) Furtak, T. E. *J. Electroanal. Chem.* **1983**, *150*, 375−388.

(20) Pockrand, I.; Otto, A. *Solid State Commun.* **1981**, *38*, 1159−1163.

(21) Buncick, M. C.; Warmack, R. J.; Ferrell, T. L. *J. Opt. Soc. Am. B* **1987**, *4*, 927−933.

(22) Moody, R. L.; Vo-Dinh, T.; Fletcher, W. H. *Appl. Spectrosc.* **1987**, *41*, 966−970.

(23) Grabar, K. C.; Freeman, R. G.; Hommer, M. B.; Natan, M. J. *Anal. Chem.* **1995**, *67*, 735−743.

(24) Freeman, R. G.; Grabar, K. C.; Allison, K. J.; Bright, R. M.; Davis, J. A.; Guthrie, A. P.; Hommer, M. B.; Jackson, M. A.; Smith, P. C.; Walter, D. G.; Natan, M. J. *Science* **1995**, *267*, 1629−1632.

(25) Grabar, K. C.; Smith, P. C.; Musick, M. D.; Davis, J. A.; Walter, D. G.; Jackson, M. A.; Guthrie, A. P.; Natan, M. J. *J. Am. Chem. Soc.* **1996**, *118*, 1148−1153.

(26) Chumanov, G.; Sokolov, K.; Cotton, T. M. *J. Phys. Chem.* **1996**, *100*, 5166−5188.

(27) Liao, P. F.; Bergman, J. G.; Chemla, D. S.; Wokaun, A.; Melngailis, J.; Hawryluk, A. M.; Economou, N. P. *Chem. Phys. Lett.* **1981**, *82*, 355.

(28) Bergman, J. G.; Chemla, D. S.; Liao, P. F.; Glass, A. M.; Pinczuk, A.; Hart, R. M.; Olson, D. H. *Opt. Lett.* **1981**, *6*, 33−35.

(29) Martin, C. R. *Science* **1994**, *266*, 1961−1965.

(30) Treichel, D. A. Ph.D. Thesis, Northwestern University, Evanston, IL, 1991.

(31) Van Duyne, R. P.; Haller, K. L.; Altkorn, R. I. *Chem. Phys. Lett.* **1986**, *126*, 190.

(32) Haller, K. L. Ph.D. Thesis, Northwestern University, Evanston, IL, 1988.

(33) SERS from colloidal Ag particles has been observed under a spectroscopic microscope. However, the detected signal might result from a cluster of particles since higher resolution images of the observed spots were not reported. See, for example, (a) Emory, S. R.; Nie, S., Pittsburgh Conference, 1996 Meeting Abstract, and (b) Vlckova, B.; Gu, X. J.; Tsai, D. P.; Moskovits, M. *J. Phys. Chem.* **1996**, *100*, 3169−3174.

(34) Wardell, J. L. In *The Chemistry of the Thiol Group*; S. Patai, Ed.; Wiley: New York, 1974; p 186.

(35) Bain, C. D.; Troughton, E. B.; Tao, Y.-T.; Evall, J.; Whitesides, G. M.; Nuzzo, R. G. *J. Am. Chem. Soc.* **1989**, *111*, 321−335.

(36) Tsen, M.; Sun, L. *Anal. Chim. Acta* **1995**, *307*, 333−340.

(37) Sonnenfeld, R.; Schneir, J.; Hansma, P. K. In *Modern Aspects of Electrochemistry*; R. E. White, J. O'M. Bockris, B. E. Conway, Eds.; Plenum: New York, 1990.

(38) Ross, C. B.; Sun, L.; Crooks, R. M. *Langmuir* **1993**, *9*, 632−636.

(39) Schoer, J. K.; Ross, C. B.; Crooks, R. M.; Corbitt, T. S.; Hampden-Smith, M. J. *Langmuir* **1994**, *10*, 615−618.

(40) Schoer, J. K.; Zamborini, F. P.; Crooks, R. M. *J. Phys. Chem.* **1996**, *100*, 11086−11091.

(41) Hsu, T. *Ultramicroscopy* **1983**, *11*, 167.

(42) Schott, J. H.; White, H. S. *Langmuir* **1992**, *8*, 1955−1960.

(43) Johnson, D. C.; LaCourse, W. R. *Anal. Chem.* **1990**, *62*, 589A-596A.

(44) The Ag particles shown in Figures 4 and 5 were deposited at 500 and 470 mV, respectively. These values are higher than the theoretical threshold of 425 mV. We think that the difference is caused by liquid junction potential and other factors associated with a non-ideal reference electrode.

(45) Butt, H.-J.; Berharz, B. *Langmuir* **1995**, *11*, 4735−4741.

(46) Keller, D. *Surf. Sci.* **1991**, *253*, 353.

(47) Albrecht, T. R.; Akamine, S.; Carver, T. E.; Quate, C. F. *J. Vac. Sci. Technol. A* **1990**, *8*, 3386−3396.

(48) Sondag-Huethorst, J. A. M.; Fokkink, L. G. J. *Langmuir* **1995**, *11*, 4823−4831.

(49) Sun, L.; Crooks, R. M. *Langmuir* **1993**, *9*, 1951−1954.

(50) Li, W.; Virtanen, J. A.; Penner, R. M. *Langmuir* **1995**, *11*, 4361−4365.

(51) Li, W.; Virtanen, J. A.; Penner, R. M. *J. Phys. Chem.* **1994**, *98*, 11751.

(52) Chan, K. C.; Kim, T.; Schoer, J. K.; Crooks, R. M. *J. Am. Chem. Soc.* **1995**, *117*, 5875−5876.

(53) Berggren, K. K.; Bard, A.; Wilbur, J. L.; Gillaspy, J. D.; Helg, A. G.; McClelland, J. J.; Rolston, S. L.; Phillips, W. D.; Prentiss, M.; Whitesides, G. M. *Science* **1995**, *269*, 1255−1257.

(54) Jackman, R. J.; Wilbur, J. L.; Whitesides, G. M. *Science* **1995**, *269*, 664−666.

(55) Chou, S. Y.; Krauss, P. R.; Renstrom, P. J. *Science* **1996**, *272*, 85−87.

(56) Masuda, H.; Fukuda, K. *Science* **1995**, *268*, 1466−1468.

(57) Note that the surface coverage n_S refers to the number of molecules per geometric surface area since the area term originates from the cross sectional area of the laser beam. In addition, if the sample surface is homogeneous over a scale of beam size, then I_R depends only on the laser power P_L, but not on the area of illumination.

(58) In eq 3, I_{NR} was measured as the integrated intensity of the 992 cm^{-1} band from a 1-mm thick benzene film, and $\sigma'_{NR} = 7.1 \times 10^{-30}$ cm^2 sr^{-1} as reported in Trulson, M. O.; Mathies, R. A. *J. Chem. Phys.* **1986**, *84*, 2068−2074.

(59) NA, the numerical aperture, is sin θ_{max} in air, where θ_{max} is the angle between the optical axis and the marginal ray entering the objective. In comparison, $\Omega = \pi(\tan\theta_{max})^2$.

(60) The integrated intensity of the C═C stretching bands from 1-mm thick 0.14 M *t*-4MMS solution was compared with the intensity of the 992 cm^{-1} band from 1-mm thick neat benzene. Thus, $n_F = 6.74 \times 10^{20}$ molecules/cm^2 for benzene, and $n_F = 8.32 \times 10^{18}$ molecules/cm^2 for *t*-4MMS.

(61) We obtained this value by ignoring the local surface roughness and assuming a closely-packed SAM of $(\sqrt{3} \times \sqrt{3})$R30 lattice on an Ag(111) surface. The $(\sqrt{3} \times \sqrt{3})$R30 lattice distance can be calculated from the nearest neighbor distance of an Ag fcc crystal (2.89 Å).

(62) The laser spot size was measured following the method in ref 32. The measurement uncertainty is primarily determined by the resolution of the one-dimensional micrometer (0.1 μm) used in the measuring apparatus.

(63) We may define the upper limit as the enhancement factor in eq 4 when the noise is comparable to the signal, i.e., $I_{SR} = I_{NOISE}$. The measured spectrum baseline noise is about 1 count per second per mW of incident power.

(64) Baranovic, G.; Meic, Z.; Gusten, H.; Mink, J.; Keresztury, G. *J. Phys. Chem.* **1990**, *94*, 2833−2843.

(65) Since n_S refers to the surface coverage per geometric area, it should be equal to the monolayer coverage multiplied by a geometric factor. The factor is simply equal to the ratio of the particle's surface area to its projected geometric area, i.e., $4\pi r^2/\pi r^2 = 4$ for spherical particles.

(66) Zeman, E. J.; Schatz, G. C. *J. Phys. Chem.* **1987**, *91*, 634−643.

(67) Blatchford, C. G.; Campbell, J. R.; Creighton, J. A. *Surf. Sci.* **1982**, *120*, 435−455.

(68) Freeman, R. G.; Hommer, M. B.; Grabar, K. C.; Jackson, M. A.; Natan, M. J. *J. Phys. Chem.* **1996**, *100*, 718−724.

(69) Gersten, J. I.; Nitzan, A. *Surf. Sci.* **1985**, *158*, 165−189.

(70) Laor, U.; Schatz, G. C. *Chem. Phys. Lett.* **1981**, *82*, 566−570.

(71) Wokaun, A.; Gordon, J. P.; Liao, P. F. *Phys. Rev. Lett.* **1982**, *48*, 957−960.